Numerical/experimental impact events on filament wound composite pressure vessel

Giovanni Perillo[1*], Frode Grytten[2], Steinar Sørbø[3], Virgile Delhaye[1]

[1] *SINTEF Material and Chemistry Department of Material and Structural Mechanics – N-7491 Trondheim – Norway*
[2] *SINTEF Material and Chemistry Department of Composite and Polymer – Oslo – Norway*
[3] *SINTEF Raufoss Manufacturing – Raufoss – Norway*

Abstract

Impacts on pressure vessels, produced by winding glass fibre with vinyl ester resin over a polyethylene liner, were numerically and experimentally investigated in the current work.

Pressure vessels were experimentally tested under low velocity impact loads. Different locations and incident energies were tested in order to evaluate the induced damage and the capability of the developed numerical model.

An advanced 3-D FE model was used for simulating the impact events. It is based on the combined use of interlaminar and intralaminar damage models. Puck and Hashin failure theories were used to evaluate the intralaminar damages (matrix cracking and fibre failure). Cohesive zone theory, by mean of cohesive elements, was used for modelling delamination onset and propagation.

The experimental impact curves were accurately predicted by the numerical model for the different impact locations and energies. The overall damages, both intralaminar and interlaminar, were instead slightly over predicted for all the configurations.

The model capabilities to simulate the low velocity impact events on the full scale composite structures were proved.

Keywords: *B. Impact behaviour, C. Finite element analysis (FEA), D. Mechanical testing, E. Filament winding,*

1. Introduction

Composite materials are becoming more and more attractive for several different applications mainly due to the corrosion properties and weight saving capabilities. Nowadays a very popular commercial application of composite is represented by pressure vessel.

In the last decades, filament winding composites (both carbon and glass fibre) have been progressively replacing metal for pressurized vessels [1] in both high tech and commercial applications. The increasing use of composite, coupled with the design complexly of such material, is increasing the demand of specialized tools capable to simulate the structural behaviour of these components reducing the necessity of expensive tests.

For pressure vessel, one of the most critical safety issues is the failure induced by low velocity impact of foreign objects (always happening during the production and/or in the service life). These events can severely affect the structural integrity leading to dangerous situations. According to the standard EN 14427 [2], the ability of the vessel design to withstand loadings other than internal pressure need to be demonstrated by a series of experimental impact/dropping tests. These need to be performed on both the cylindrical and the dome section of the vessel in order to verify the most critical part of the structure. This is one of the most severe design requirements that need to be fulfilled for their commercialization. In this

*Correspindign author - Email: giovanni.perillo@sintef.no Telephone number: (+47) 47160974

scenario, the availability of numerical tools capable of properly simulate the impact event can reduce the experimental costs during the design phase. Even more, the composite layup/constituents and more generally the complete vessel design can be simply numerically optimized in order to fulfil the same safety requirements but reducing the production cost (high benefit considering the amount of produced units).

The effect of impact on filament wound structures is still not well understood and even more its numerical simulation is extremely complicated. A first numerical investigation was conducted by Changliang et al. [3] where 3D finite element (FE) model was used to evaluate the impact induced damage on metal liner composite vessel. Parametric analyses, varying the incident energy and the internal pressure, were carried out. Matrix cracking and delamination were evaluated by the use of Chang and Chang criteria [4]. Even if the results were consistent with the physical behaviour, the model accuracy was not verified against experimental data.

There is more available literature concerning the impact on filament wound composite structures (not specifically for pressure vessel). Alderson and Evans [5, 6] compared the damage induced by an impact event against simple static tests on thin filament wounded E-Glass/Epoxy tubes with a ±55° winding angle. They observed that the first modes of damage were always delamination and local crushing, just like for carbon composites [7]. Geometrical effects, such as boundary conditions and curvature are also important for impact induced damage [3,4]. Christoforou et al. [8] and Curtis et al. [9] investigated the influence of impact damage on the burst pressure for thin composite pipes. Both researches showed a drastic reduction of the pressure resistance due to impact damage. Ozdil et al. [10] investigated the influence of defects and impact damage on the external (implosion) pressure. It was shown that the damage produced by low energy impact leads to a reduction of the implosion pressure. Tarfaoui et at. [11-14] carried out an extensive test program, arriving at the same conclusion that the impact damage reduces considerably the implosion pressure. Moreover, the same author [15] was able to predict the impact curves with good accuracy, using finite element model with progressive failure analysis (based on Hashin failure criterion [16]). The model was not intended to predict the onset and the propagation of delamination. A more complex numerical model was used by Zou et al. [17] and Li et al. [18] that investigated the impact induced damage on filament wounded pipes. A progressive interlaminar approach was used, based on a stress criterion for the damage onset and principles of fracture mechanics for the damage propagation. The numerical predictions showed good agreement with the experimental data for both the size and the shape of delaminations.

No numerical models (with the simultaneous evaluation of interlaminar and intralaminar damages) have been used so far, to simulate the impact event/damage on filament wound component/structures.

In the current work several experimental impact tests were carried out on commercial filament wound composite vessel with internal polyethylene liner. Different impact configurations (energy and position of impact) were experimentally testes in a fully instrumented drop weight machine. All the tests were also recorded by a high speed camera. The experimental tests were then accurately simulated using a commercial finite element software coupled with an advanced damage model for composite material. This, developed for the commercial software ABAQUS Explicit [19], was based on a combination of: interlaminar (by means of the cohesive zone approach) and intralaminar models (by a combination of Puck [20-22] and Hashin [16] strength based failure criteria).

2. Methodology

2.1. Pressure vessels

All the experimental/numerical tests were performed on filament wound pressure vessels. The vessels were produced with an internal polyethylene liner covered by E-Glass fibre and vinyl ester resin composite produced by filament winding.

The vessels were also equipped with an inlet/outlet brass valve for the pressurization. For safety reason, the samples were not pressurized during the impact tests; a low overpressure was anyway present (approximately 2 bar) in order to keep the proper sample's shape.

The vessels presented a height of 460mm (including the main valve), maximum diameter of 300mm (measured in the central section) and a engineering/nominal thickness varying from 1.3mm to 3.4mm (central and dome section respectively). More details about the layup orientations in the different sections of the vessel are reported in the following sections.

2.2. Material properties

The vessels were made of three distinct parts: the internal liner, the external composite shell and the main valve. In order to proper simulate the impact events, the material properties of the different parts were required.

The properties of the internal liner and the valve were provided by the material supplier and reported in Table 1. The properties of the composite were instead measured for the specific material/production process by means of a full campaign of experimental tests. Split disk [23] and biaxial [24-26] tests were carried out in order to evaluate the material moduli and strengths. The results of the material characterization are reported in the Table 1.

Currently, no test techniques are available for the evaluation of the critical fracture toughness energies (G_{Ic}, G_{IIc} and G_{IIIc}), fundamental for the evaluation of the interlaminar damage (delamination). A first attempt to evaluate these values was carried out by the author and reported in [27]. The curved double cantilever beam test technique used in [27] was not usable in the present work for the specific material. The data used here (reported in Table 1) were defined using data evaluated on similar material previously characterized.

2.3. Experimental Impact Tests

Following the general suggestion of the EN 14427 [2] standard, two different configurations were defined for the impact tests.

- ***Central section***: the impact position was located in the cylindrical section of the vessel (more details in Figure 1). This section is characterized by the presence of both helical and hoop layers. The impact in this region could damage the hoop layer (fibre failure) with the consequent reduction of the maximum burst pressure of the vessel. The correct simulation of the damage in this section is fundamental to improve the vessel safety.
- ***Dome section (angle of 45°)***: the impact position was located on the dome section (same side of the valve) of the vessel. The samples were inclined with an angle of 45^0 (respect to the cylindrical axe) using a custom fixture (see Figure 1). This configuration was selected in order to evaluate the model capability to simulate the damage onset and propagation in a region where the fibre orientation is continuously varying. This results in an increase of the simulation complexity that can affect the model accuracy.

As reported before, for safety reason, during the impact the vessels were pressurized at approximately 2 bars. Further work should be done in order to evaluate the influence of the internal pressure on the impact damage and the model capabilities.

All the tests were carried out in a full instrumented Instron CEAST 9350 drop weight machine with automatic anti-rebound system. The machine was equipped with accelerometer, embedded directly in the impactor, in order to measure the impact data. The data were recorded by a high frequency acquisition system, CEAST DAS 64k, using a sampling rate of 1000k Hz for a total time of 20ms. All the tests were also recorded with a high speed camera in order to visually evaluate the damage initiation and propagation (on the external part of the vessel). A FASTCAM SA1.1 camera, at 15000 frames per second, was used. The camera was triggered directly on the impactor movement by a speed sensor (placed just before the impactor got in contact with the sample).

All tests were carried out using a spherical impactor with a diameter of 16mm and mass of 5kg that was kept constant for all the tests. The mass was selected in order to use the lower weight but fulfilling the energy requirements (to produce a consistent damage) without exceeding the machine capability. A set of preliminary impact tests was carried out to evaluate the induced damage at several impact energies. The selected energies were defined in order to produce a consistent damage (mainly matrix cracking and delamination) without affecting the sealing of the vessel. This choice was done in order to produce damage (similar to a dropping of a tool during the vessel handling) not noticeable by a depressurization of the vessel (a leakage is simply detected). The presence of a barely visible damage (BVID) is the most critical situation for the vessel safety.

A common problem for filament wound structures [1] is the possibility of small asymmetry of the dome section (mainly generated during the placement process of the helical layers). For this reason, a preliminary investigation was carried out to evaluate the influence of the impact position (at the dome section along the sample circumference). The results showed a variation of approximately 10% for the impact results (maximum force and total impact time) at the different impact points (four points tested). The weakest area was used for all the further tests here reported.

A summary of all the different test configurations is given in Table 2.

2.4. Damage model for composite material

An advanced numerical model was developed to simulate the damage onset and development in the external composite part of the vessel. The damage model, based on the combined use of Puck [20-22] and Hashin [16] failure criteria, was used to evaluate the intralaminar damage (matrix cracking and fibre failure). The model was implemented by a user defined subroutine to be used in the commercial FE software Abaqus 6.11 [19]. The onset and propagation of interlaminar damage (delamination) was evaluated by the cohesive zone model (CZM) implemented by cohesive elements.

More details about the damage models and their basic assumptions are reported in the following paragraphs.

2.4.1. Intralaminar damage model

The intralaminar damage model is based on the combined used of two different strengths based failure criteria. The classical Hashin criterion [16] was used for the evaluation of the fibre failure, while the innovative Puck criterion [20-22] was used for the matrix cracking. The Puck criterion for fibre failure

was not used due to the complexity to measure the required material properties (more details in [20-22]). Both methods were applied on the ply level using a user defined material model coded in a VUMAT subroutine, written in FORTRAN, for Abaqus/Explicit [28]. The damage is evaluated at each integration point at each time step of the simulation for all the elements.

Hashin criterion

According to the Hashin criterion [16], the fibre failure occurs when the parameter $f_{ff} \geq 1$. f_{ff} is evaluated by equation (1) different for tension and compression loads condition:

$$f_{ff} = \begin{cases} \left(\frac{\sigma_1}{X_t}\right)^2 + \frac{1}{{S_{12}}^2}(\tau_{12}^2 + \tau_{13}^2) & for\ \sigma_1 \geq 0 \\ \left(\frac{\sigma_1}{X_c}\right)^2 & for\ \sigma_1 < 0 \end{cases} \quad (1)$$

where σ_1 is the stress in the direction of fibre, τ_{12} and τ_{13} are the in-plane and out-of-plane shear stresses respectively. X_t and X_c are the tension and compression strengths in the direction of the fibre. S_{12} is the in plane shear strength. More details about this failure theory can be found in [16].

Puck criterion

The Puck failure criterion [20-22] is an interactive stress-based criterion applicable for unidirectional (UD) composite lamina. The matrix failure criterion is based on the assumption that failure is created only by the stresses that act on the fracture plane (σ_n, τ_{nl} and τ_{nt}) inclined at θ_{fp} to the material plane (see Figure 2). The normal and shear stresses acting on this plane are calculated by rotating the three-dimensional stress tensor from the material coordinate system to the fracture plane using classical tensor transformations. The matrix failure is then described by an inter-fibre failure criterion (see equation 2) that is only a function of the stresses acting on the fracture plane. Failure is reached when $f_{iff} \geq 1$:

$$f_{iff} = \begin{cases} \sqrt{\left[\left(\frac{1}{R_\perp} - \frac{P_{\perp\psi}^+}{R_{\perp\psi}}\right)\sigma_n(\theta)\right]^2 + \left(\frac{\tau_{nt}(\theta)}{R_{\perp\perp}}\right)^2 + \left(\frac{\tau_{nl}(\theta)}{R_{\perp\parallel}}\right)^2} + \frac{P_{\perp\psi}^+}{R_{\perp\psi}}\sigma_n(\theta) & for\ \sigma_n \geq 0 \\ \sqrt{\left(\frac{\tau_{nt}(\theta)}{R_{\perp\perp}}\right)^2 + \left(\frac{\tau_{nl}(\theta)}{R_{\perp\parallel}}\right)^2 + \left[\left(\frac{P_{\perp\psi}^-}{R_{\perp\psi}}\right)\sigma_n(\theta)\right]^2} + \frac{P_{\perp\psi}^-}{R_{\perp\psi}}\sigma_n(\theta) & for\ \sigma_n \leq 0 \end{cases} \quad (2)$$

where $R_\perp$ is the failure resistance perpendicular to the fibers, $R_{\perp\psi}$ and $R_{t\parallel}$ are the shear resistances, and $P_{\perp\psi}^+$ and $P_{\perp\psi}^-$ are the slope parameters representing the internal friction effects in the Mohr-Coulomb failure criterion (more details in [22]). The parameters presented before can be calculated using the following expressions:

$$\frac{P_{\perp\psi}^+}{R_{\perp\psi}} = \frac{P_{\perp\perp}^+}{R_{\perp\perp}}(\cos\psi)^2 + \frac{P_{\perp\parallel}^+}{R_{\perp\parallel}}(\sin\psi)^2 \qquad \frac{P_{\perp\psi}^-}{R_{\perp\psi}} = \frac{P_{\perp\perp}^-}{R_{\perp\perp}}(\cos\psi)^2 + \frac{P_{\perp\parallel}^-}{R_{\perp\parallel}}(\sin\psi)^2$$

$$(\cos\psi)^2 = \frac{\tau_{nt}^2(\theta)}{\tau_{nt}^2(\theta) + \tau_{nl}^2(\theta)} \qquad (\sin\psi)^2 = \frac{\tau_{nl}^2(\theta)}{\tau_{nt}^2(\theta) + \tau_{nl}^2(\theta)} \quad (3)$$

$$R_\perp = Y_t \qquad R_{\perp\parallel} = S_{21} \qquad R_{\perp\perp} = \frac{Y_c}{2(1 + P_{\perp\perp}^-)}$$

where Y_t and Y_c are the tension and compression in-plane material strengths, respectively, in the direction perpendicular to the fibres. In addition to the standard material parameters, special Puck parameters are needed. The measurement of these parameters requires complicated multi-axial testing. However, Puck

recommends using the default parameters reported in Table 3. The default parameters were used in this study.

The damage propagation was simulated by a progressive failure analysis. When failure is predicted in a particular position of the composite, the elements of the stiffness matrix are reduced according to the failure type predicted by the failure criterion. In the case of fibre failure, all of the components of the stiffness matrix are reduced to zero. In the case of matrix cracking, only the transverse and shear components are reduced. In both cases, the out of plane component of the stiffness matrix is kept equal to the undamaged one to avoid any unnatural penetration. This degradation modelling is a simple and reasonable approach that does not need any further testing to establish properties after first damage.

2.4.2. Interlaminar damage model

The delamination initiation and propagation was simulated using the cohesive zone model (CZM) approach. The model is based on the assumption that a thin material, with a different constitutive law, is present between the different composite layers. This interface connects the different layers, and it is simulated by thin cohesive elements placed between each layer where the delamination is expected to propagate. Delamination can propagate only between differently oriented layers [29] due to the interlaminar shear stresses, and thus, the delamination path is known a priori.

The classical bi-linear traction-separation laws based on the total dissipated energies was used in the cohesive zone elements. The cohesive behaviour was defined directly in terms of a traction-separation law. The following assumptions were used for the cohesive model:

- Undamaged behaviour based on a linear elastic traction separation law
- A quadratic nominal stress criterion was used for the evaluation of the damage initiation
- Linear damage evolution law based on the total dissipated energies
- Linear degradation law function of the dissipated energy
- The Benzeggagh-Kenane [30] (BK) law for the mixed opening mode (mode I plus mode II or III)
- The material properties of the interface can be considered matrix dominated. For this reason the following assumptions were used:
    - Normal modulus $K_{nn}=E_2$
    - Normal strength $t_n=Y_t$
    - Equal shear moduli in both directions $K_{ss}=K_{tt}=G_{12}$
    - Equal shear strengths in both directions $t_s=t_t=S_{12}$

The parameters K_{nn}, K_{ss}, K_{tt}, t_n, t_s and t_t are the stiffnesses and strengths of the CZM model, as described in detail in the ABAQUS manual [19].

2.5. Numerical implementation of the impact tests

The experimental impact tests reported before were simulated using the commercial finite element software Abaqus Explicit 6.11 [19] coupled with the numerical damage model previously described.

The impact test was numerically modelled assembling several parts as schematically reported in Figure 3. The modelling details of each part will be discussed in the following paragraphs.

2.5.1. External composite

The external composite part of the vessel is produced by filament winding using the material described before. Due to the production process and the sample geometry, the layup definition is trivial. The dome

section presents a continuous variation of the fibres orientation that needed some simplifications in order to be modelled. Several trials were done to find the optimum compromise between the model complexity and the simulation accuracy. The best was obtained dividing the dome in eight subsections in which the layup orientation was step by step varied (each subsection presented a fix layup/orientation). A schematic drawing is reported in Figure 4.

The damage model (presented in the previous section) required to model each composite ply separately placing the cohesive interfaces between the plies. Each ply was discretized using two (in the thickness direction) standard continuum solid hexahedral element C3D8R [19] with eight nodes and reduced integration scheme. The intralaminar damage model, coded in a VUMAT subroutine, was integrated in the elements and evaluated at each time increment for each integration point. The hourglass, by means of the enhanced method, and the distortion controls were used for all of the elements [19].

The interfaces between differently oriented plies were discretized using the cohesive element COH3D8 [19] defined with the classical bilinear traction separation law (more details in the previous section). Each interface was modelled with a thickness of 0.01 mm, which was deducted from the thickness of the adjacent layers to obtain the same total laminate thickness. The cohesive thickness of 0.01 mm was defined to get the best compromise between the computational time and the reduction of the global laminate stiffness related to the presence of the cohesive interfaces.

In order to reduce the computational time, only small part of the vessel around the impact zone was discretized using the approach presented before (C3D8R + COH3D8 elements with the damage model implemented). This area was defined after the evaluation of induced damage on the experimental impacted samples. In Figure 5, the different areas are showed for both configurations. The remaining part of the external composite part of the vessel was modelled with purely elastic (no damage) eight nodes reduced integrated continuum shell elements, SC8R [19], with a layered section. These elements were preferred to the classical shell S4R elements in order to keep a low computational cost without affecting the model accuracy. The precision of the used contact algorithm (more details in the following paragraphs) could have been affected using shell elements [19].

2.6. Impactor, base, internal liner and valve

The impactor and the base were simulated as infinite rigid surface by mean of R3D4 elements [19]. For both two impact configurations, the geometry of the base was modified in order to reduce the computational cost of the contact simulation. A V-shaped base with a 33° angle was used.

The internal liner was modelled with one (through the thickness direction) continuum shell element SC8R [19]. The valve was instead modelled with standard solid element C3D8R [19]. For both parts, linear elastic material models were used with the properties reported in Table 1.

2.7. Boundary conditions and contact algorithm

The boundary conditions were defined in order to better simulate the experimental tests. A resume scheme of them is reported in Figure 6 for both two impact configurations.

The general contact algorithm, available in Abaqus Explicit 6.11 [19], was used between all the surfaces. The normal behaviour was defined by hard contact law [19] while the Coulomb model was selected for the friction formulation [19]. No experimental measurements were conducted to evaluate the friction coefficient between the different involved materials (impactor/composite, composite/composite and

composite/base). Several studies investigated the friction coefficient between metal and composite and composite/composite [31, 32]. In the present work, an average friction coefficient of μ=0.3, was used for all of the implemented contacts with no distinctions.

2.8. Mesh details

The element sizes of the different model parts need to be carefully defined in order to obtain accurate results [33]. For both two configurations a very fine mesh was used. Moreover, due to the complexity of the layup and the curved surface, the composite and cohesive layers where modelled with shared nodes [19] (instead of modelling the different parts individually and connect them by tie constrains). This modelling technique did not allow the use of a finer mesh only for the cohesive interfaces (reducing the computation cost of the simulation). For this reason, both the cohesive interfaces and composite layers, were discretized with elements of an approximately in plane dimension of 1x1mm (two elements in the thickness direction for the composite layers and one element for the cohesive interfaces).

More coarse mesh was used in the remaining part of the sample. Elements of approximately 3mm length were used for the remaining part of the external composite and internal liner (one element in the thickness direction). Elements of 0.5x0.5mm were used for the impactor and 10x10mm for the base.

The final element sizes previously reported were defined after a preliminary mesh sensitivity analysis. The different meshes (varying the in plane elements dimension) were compared in order to obtain the best compromise between the computational time and the results accuracy (evaluated by the comparison of the delamination shape and impact curve against the experimental data).

3. Results and discussion

3.1. Experimental impact tests

At least three samples were tested for each configuration and impact energy. As reported in Figure 7, the impact curves showed a very good reproducibility with a low scatter (<8%). The data for each set of tests were averaged and are reported in Figure 8.

The impact curves presented a very similar behaviour. The initial response is almost linear for all the different configurations (dome and central section at different energy) followed by a reduction of the curve slope representing the damage initiation (matrix cracks and delamination). Slightly different the behaviour at higher impact energies (60J and 100J) where a drastic drop of the contact force is showed after the initial elastic response. This behaviour can be related to the different type of failure happening during the impact. Analysing the recorded videos, it was possible to clearly see a small amount of fibre failure happening at early stage (in correspondence of the drop in the force curve) of the impact event. For lower energies (20J and 40J) the fibre failure occurred later in correspondence of the maximum reached displacement.

Due to the transparent nature of the used material, the induced damage was evaluated by the back light technique [5, 34, 35] for the different configurations. The induced damage showed quite a large variation for both size and shape (for the same configuration/energy). For this reason no representative images are reported here.

From a rough evaluation, the delamination and matrix cracks resulted anyway proportional to the incident impact energy. A large amount of fibre failure was visible the impact on the central section of the vessel. In this case the hoop layer, placed on the outer surface of the vessel, reported a single vertical

(transverse to the fibre direction) crack (fibre failure) whose length increased with the impact energy. Fibre failures were also visible for the impact on the dome section but only at the higher impact energies (60J and 100J).

3.2. Numerical impact simulations

The experimental impact tests, were simulated using the commercial FEM software Abaqus 6.11 [19]. In Figure 9 and Figure 10 the numerical/experimental data are reported and compared for the different configurations/impact energies.

The results showed a quite good accuracy of the numerical model to predict the experimental impact behaviour. The maximum impact force, the total impact time, the maximum displacement and the initial elastic response were accurately simulated.

In Figure 11 the numerically predicted and experimentally measured absorbed energies are reported for the different configurations. All the plots shown in Figure 11 are normalized by the maximum incident impact energy. The simulations were able to predict the kinetic energy evolution quite well. Small discrepancy is showed for the data of central impact but the general trend is anyway well predicted.

The overall interlaminar and intralaminar damages were evaluated for the different configurations and reported in Figure 12 and Figure 13 (it was not possible to report the report the experimental damage). For the impact on the central section, the overall interlaminar and intralaminar damage showed a reasonable pattern with a slightly overestimation of the total size. More pronounced is the overestimation for the impact on the dome section. The error of the numerical model can be related to several factors. Mainly the lack of information about the interlaminar fracture toughness could have affected the overall delaminated area. This coupled with the complexity of the geometrical model for the dome section, could have increased the mismatch. The matrix cracks overestimation can be instead related to the used material properties or geometrical errors of the numerical model. The material properties were evaluated on the same constituents and the same production process but with different production parameters in order to be made in a lab scale facility. This could have affected the values reducing the model accuracy. Moreover, due to the industrial production process, the vessel showed consistent local variation of the thickness of the external composite section. The thickness in the numerical model was defined as an averaged value between the different measured ones for each section. In addition, the implemented failure model could be a source of error. The elements of the stiffness matrix were reduced when damage was predicted (matrix cracking and fibre failure). A better modelling method may be the continuum damage approaches [36-38], but they were not implemented here. These models require material data (the dissipated energies during the damage) that are difficult to obtain. The increased test effort may be worth for high tech applications, but it can usually not be justified for the applications investigated here. The general variability of the properties of filament wound composite would also mask the benefits of additional testing.

Overall, the numerical impact curves (force-time and force-displacement reported in Figure 9 and Figure 10) showed very good agreement with the experimental data, indicating that damage was modelled with sufficient accuracy.

4. Conclusion

Impacts on full scale composite pressure vessel were numerically and experimentally investigated.

The numerical simulations were carried out using an advanced 3-D FE model, with the simultaneously use of intralaminar and interlaminar damages theories. The Hashin failure criterion was used for the evaluation of fibre failure and the Puck criterion for matrix cracks. Delamination onset and propagation was evaluated by cohesive theory. The bilinear traction separation law, based on the critical strain energy release rates, was used. The material model was implemented in the FE software Abaqus Explicit [19] by a VUMAT subroutine.

The FE simulations were able to accurately predict the impact events. The total impact time as well as the maximum impact force was well captured for all impact configurations (different impact positions and impact energies). The induced damage was over predicted by the numerical model. This error can be related to both the inaccuracy of the used material properties, geometrical error (thickness variation was not considered in the model) and due to the implemented stiffness matrix degradation method. Higher accuracy was found for the impact energy that was predicted with less than 5% of error.

Future work should focus on the improvement of the developed damage model. A continuum damage approach, evaluating the total energy dissipated during the matrix cracking evolution, should be implemented in order to reduce the damage overestimation of the model. Overall the FE model and its failure criteria showed good accuracy for modelling impact damage on full scale composite component.

5. Acknowledgements

This work is part of the collaborative project "Composite structures under impact loading - COMPACT". The authors would like to express their thanks for the financial support by the Norwegian Research Council (grant 193238/i40) and the industrial partners. The authors would also like to thank all partners in the project for constructive discussions.

6. Reference

[1] Peters ST. Composite Filament Winding: Materials Park : ASM International; 2011.
[2] Standardization ECf. EN 14427: Transportable refillable fully wrapped composite cylinders for liquefied petroleum gases (LPG). Design and construction. 2004.
[3] Changliang Z, Mingfa R, Wei Z, Haoran C. Delamination prediction of composite filament wound vessel with metal liner under low velocity impact. Composite Structures. 2006;75(1–4):387-92.
[4] Chang F-K, Chang K-Y. A progressive damage model for laminated composites containing stress concentrations. Journal of Composite Materials. 1987;21(9):834-55.
[5] Alderson KL, Evans KE. Low velocity transverse impact of filament-wound pipes: Part 1. Damage due to static and impact loads. Composite Structures. 1992;20(1):37-45.
[6] Evans KE, Alderson KL. Low velocity transverse impact of filament-wound pipes: Part 2. Residual properties and correlations with impact damage. Composite Structures. 1992;20(1):47-52.
[7] Abrate S. Impact on composite structures.1998.
[8] Christoforou AP. Impact dynamics and damage in composite structures. Composite Structures. 2001;52(2):181-8.
[9] Curtis J, Hinton MJ, Li S, Reid SR, Soden PD. Damage, deformation and residual burst strength of filament-wound composite tubes subjected to impact or quasi-static indentation. Composites Part B: Engineering. 2000;31(5):419-33.
[10] Ozdil F, Carlsson LA, Davies P. Characterization Of Delamination Toughness Of Angle-Ply Glass/Epoxy Cylinders. Proceedings ICCM 12 - Paris. 1992.
[11] Gning PB, Tarfaoui M, Collombet F, Davies P. Prediction of damage in composite cylinders after impact. Journal of Composite Materials. 2005;39(10):917-28.
[12] Gning PB, Tarfaoui M, Collombet F, Riou L, Davies P. Damage development in thick composite tubes under impact loading and influence on implosion pressure: experimental observations. Composites Part B: Engineering. 2005;36(4):306-18.
[13] Tarfaoui M, Gning PB, Davies P, Collombet F. Scale and Size Effects on Dynamic Response and Damage of Glass/Epoxy Tubular Structures. Journal of composite materials. 2007;41(5):547-58.
[14] Tarfaoui M, Gning PB, Collombet F. Residual strength of damaged glass/epoxy tubular structures. Journal of Composite Materials. 2007;41(18):2165-82.
[15] Tarfaoui M, Gning PB, Hamitouche L. Dynamic response and damage modeling of glass/epoxy tubular structures: Numerical investigation. Composites Part A: Applied Science and Manufacturing. 2008;39(1):1-12.
[16] Hashin. Failure criteria for unidirectional composites. J Appl Mech. 1980;47:329-34.
[17] Zou Z, Reid SR, Li S, Soden PD. Application of a delamination model to laminated composite structures. Composite Structures. 2002;56(4):375-89.
[18] Li S, Soden PD, Reid SR, Hinton MJ. Indentation of laminated filament-wound composite tubes. Composites. 1993;24(5):407-21.

[19] Abaqus I. Abaqus Version 6.11 User's manual. 2011.
[20] Puck A, Kopp J, Knops M. Guidelines for the determination of the parameters in Puck's action plane strength criterion. Composites Science and Technology. 2001;62(3):371-8.
[21] Puck A, Schürmann H. Failure analysis of FRP laminates by means of physically based phenomenological models. Composites Science and Technology. 1998;58(7):1045-67.
[22] Puck A, Schürmann H. Failure analysis of FRP laminates by means of physically based phenomenological models. Composites Science and Technology. 2001;62(12-13):1633-62.
[23] ASTM. D2290-12 Standard Test Method for Apparent Hoop Tensile Strength of Plastic or Reinforced Plastic Pipe.
[24] ASTM. D5450/D5450M-12 Standard Test Method for Transverse Tensile Properties of Hoop Wound Polymer Matrix Composite Cylinders.
[25] ASTM. D5449/D5449M-11 Standard Test Method for Transverse Compressive Properties of Hoop Wound Polymer Matrix Composite Cylinders.
[26] ASTM. D5448/D5448M-11 Standard Test Method for Inplane Shear Properties of Hoop Wound Polymer Matrix Composite Cylinders.
[27] Perillo G, Echtermeyer AT. Mode I Fracture Toughness Testing of Composite Pipes. Applied Composite Materials. 2013;20(6):1135-46.
[28] Abaqus User Subroutines Reference Manual.
[29] Abrate S. Impact on composite structures. 1998;Cambridge University Press:289.
[30] Benzeggagh ML, and M. Kenane. Measurement of Mixed-Mode Delamination Fracture Toughness of Unidirectional Glass/Epoxy Composites with Mixed-Mode Bending Apparatus. Composites Science and Technology. 1996;56:439–49.
[31] Lancaster JK. The effect of carbon fibre reinforcement on the friction and wear of polymers. Journal of Physics D: Applied Physics. 1968;1(5).
[32] Schön J. Coefficient of friction of composite delamination surfaces. Wear. 2000;237(1):77-89.
[33] Turon A, Davila CG, Camanho PP, Costa J. An engineering solution for mesh size effects in the simulation of delamination using cohesive zone models. Engineering Fracture Mechanics. 2007;74:1665-82.
[34] Sutherland LS, Guedes Soares C. Effects of laminate thickness and reinforcement type on the impact behaviour of E-glass/polyester laminates. Composites Science and Technology. 1999;59(15):2243-60.
[35] Sutherland LS, Guedes Soares C. Impact tests on woven-roving E-glass/polyester laminates. Composites Science and Technology. 1999;59(10):1553-67.
[36] Maimí P, Camanho PP, Mayugo JA, Dávila CG. A continuum damage model for composite laminates: Part I – Constitutive model. Mechanics of Materials. 2007;39(10):897-908.
[37] Maimí P, Camanho PP, Mayugo JA, Dávila CG. A continuum damage model for composite laminates: Part II – Computational implementation and validation. Mechanics of Materials. 2007;39(10):909-19.
[38] Pinho STD, C. G.; Camanho, P. P.; Iannucci, L.; Robinson, P. Failure Models and Criteria for FRP Under In-Plane or Three-Dimensional Stress States Including Shear Non-Linearity. NASA Technical reports. 2005;NASA/TM-2005-213530, L-19089.
[39] Perillo G, Vedivik N, Echtermeyer A. Numerical and experimental investigation of impact on filament wound glass reinforced epoxy pipe. Journal of Composite Materials. 2014.

Table 1: Material properties
Composite properties:

Properties	Value
Fibre volume fraction	45.7%
Density	1230 kg/m^3
Elastic properties	E_1= 61.54 *GPa*; E_2= E_3*=13.93 *GPa*; G_{12}=G_{13}*=G_{23}*=1.43 *GPa;* ν_{12}=ν_{13}*=0.30; ν_{23}*=0.5;
Strength *[MPa]*	X_t=837; X_c=414; Y_t=Z_t*=25.8; Y_c= Z_c*=100.2; S_{12}= S_{13}*= S_{23}*=44.24;

**Assumed*
***Note: X is the fibre direction, Y is the matrix direction, t is for tension and c for compression; S12 is for shear*

Interlaminar properties:

Properties	Value
Elastic properties	K_{nn}*= 13.93 *GPa*; K_{ss}*= K_{tt}*= 1.43 *GPa*
Strength *[MPa]*	t_n*=25.8; t_s*= t_t*=44.24;
Fracture toughness *[N/mm]*	G_{Ic}**=0.83; G_{IIc}**= G_{IIIc}**=3.15
Mode interaction – BK	η*=1.40

**See section "Interlaminar damage model" for more detail*
***Data from similar material (E-Glass/Epoxy produced by filament winding) from [39]*

Liner properties:

Properties	Value
Density	1230 kg/m^3
Elastic properties	E= 3.5 *GPa*; ν_{12}=0.30;

Valve properties:

Properties	Value
Density	1230 kg/m^3
Elastic properties	E= 7 *GPa*; ν_{12}=0.30;

Table 2: Resume of the different impact configurations

Configuration	Impact energy [J]	Impactor mass [kg]	Impactor velocity [m/s]
Central section	20	5 Kg	2.82
	40		3.98
Dome section	20		2.82
	40		3.98
	60		4.88
	100		6.3

Table 3: Special Puck parameters from [20]

Fibre Type	$P^+_{\perp\parallel}$	$P^-_{\perp\parallel}$	$P^+_{\perp\perp}$	$P^-_{\perp\perp}$
Glass Fibre	0.30	0.25	0.20 – 0.25	0.20 – 0.25
Carbon Fibre	0.35	0.30	0.25 – 0.30	0.25 – 0.30

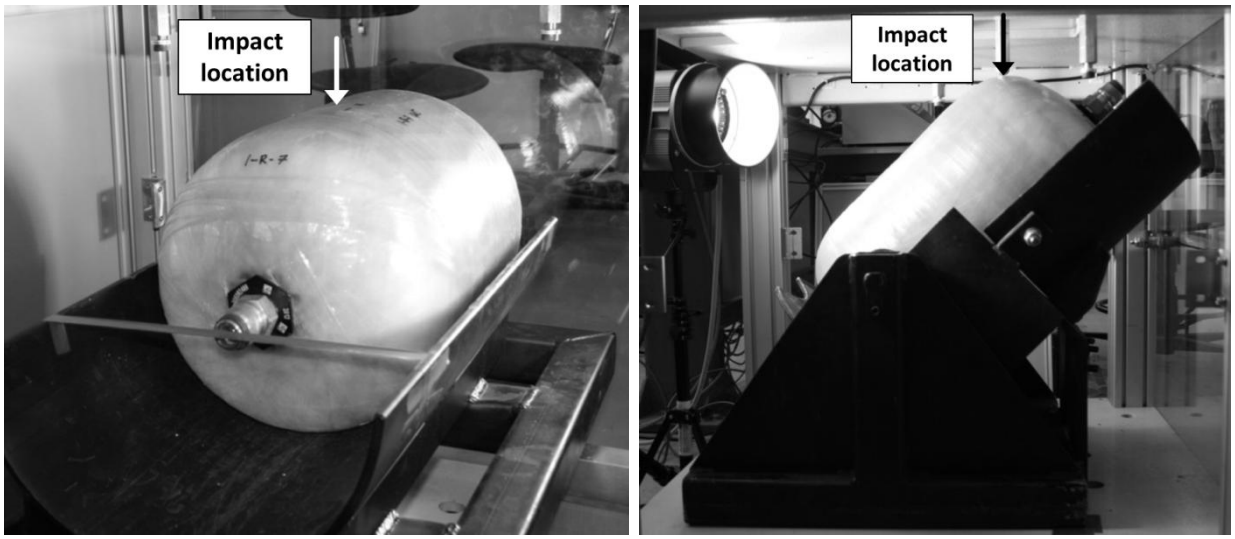

Central section Dome section

Figure 1: Test configurations

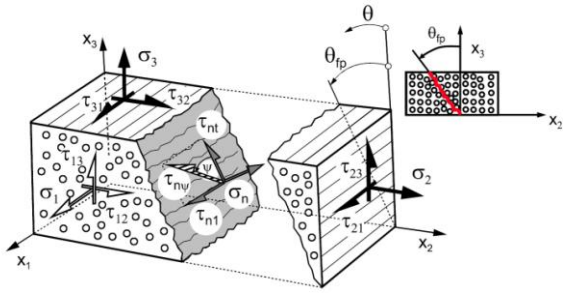

Figure 2: Puck fracture plane definition [22]

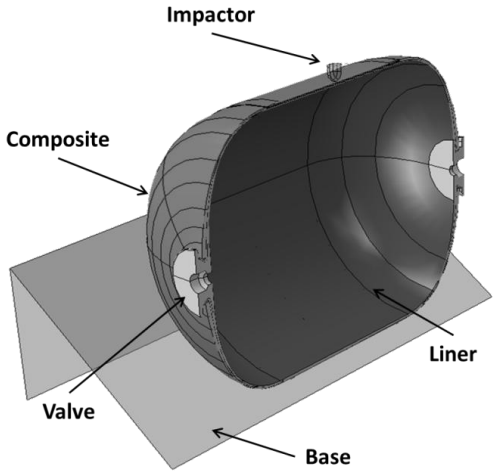

Figure 3: Different part of the model (only half of the model is reported in this figure)

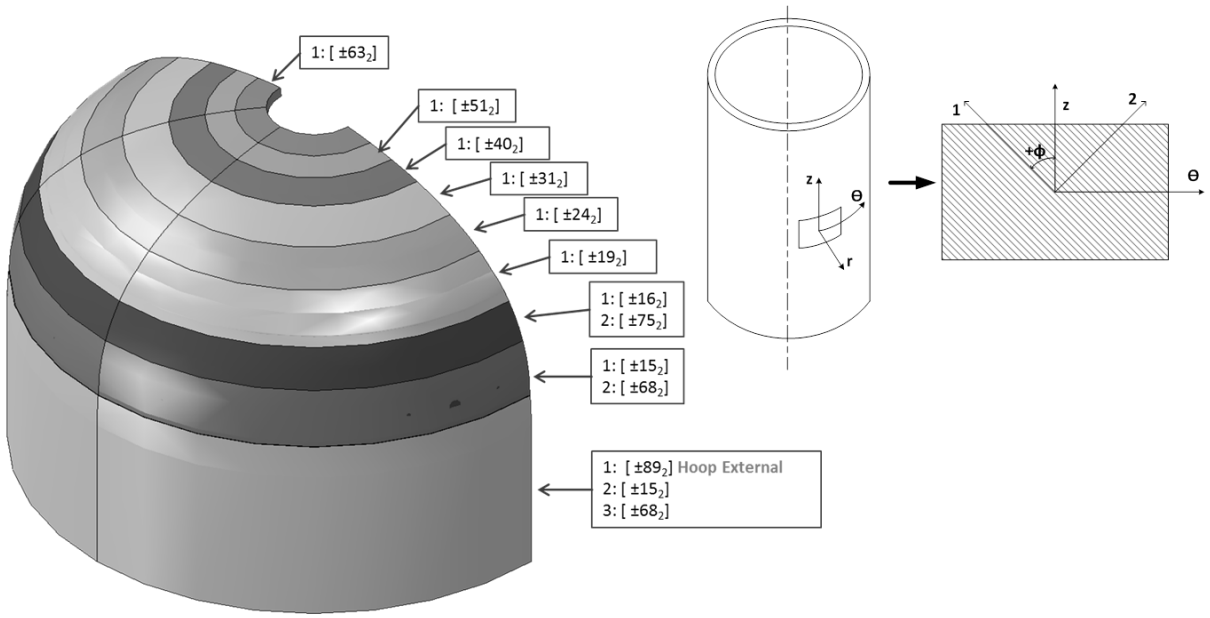

Figure 4: Used layup for finite element model with the reference coordinate system – Only a quarter of the model is reported in order to simplify the visualization

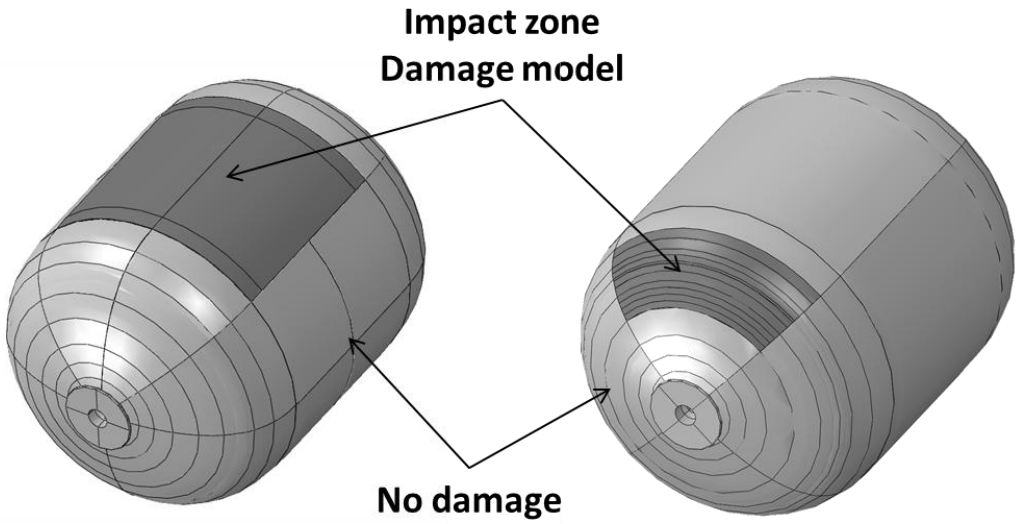

Figure 5: FEM model. In red the impact zone modelled with the developed damage model

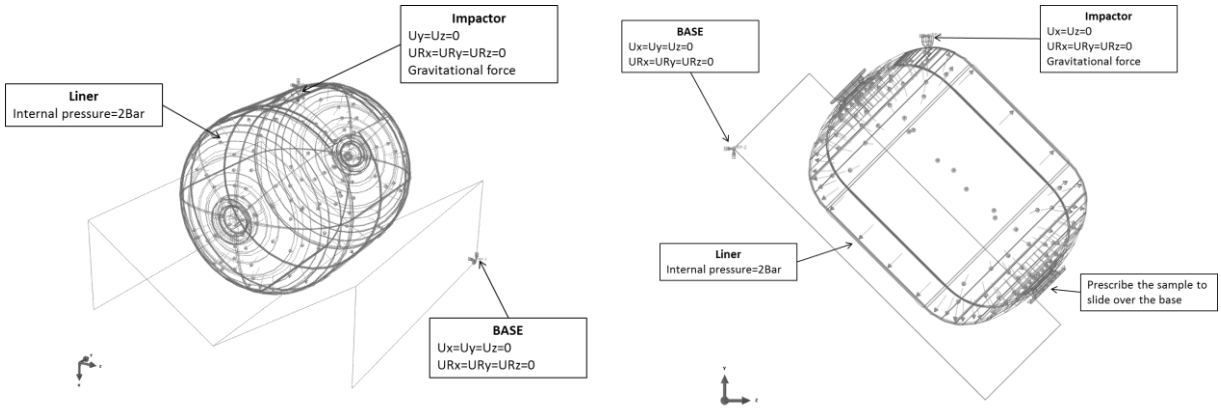

Central section impact Dome section impact

Figure 6: Model boundary conditions

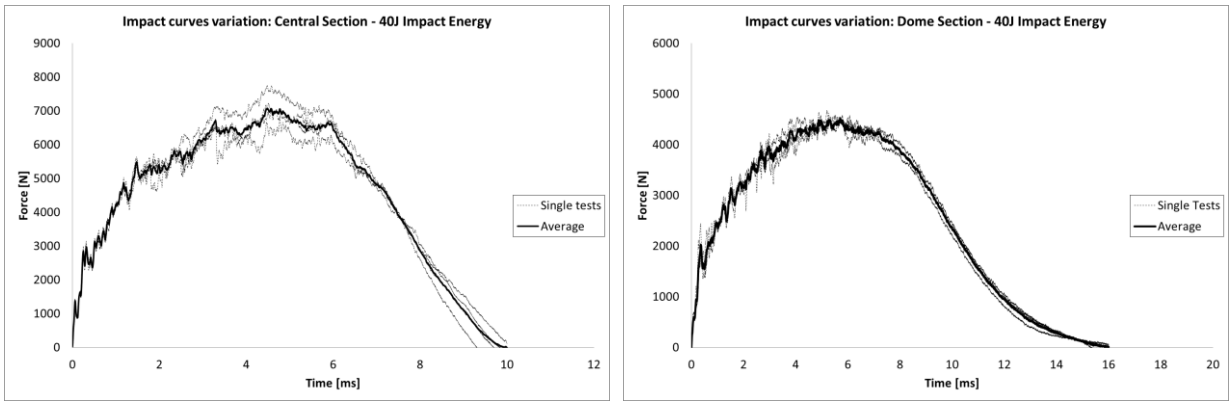

Figure 7: Example of the reproducibility of the experimental impact tests. The impact data for the single tests and the average curve are reported for the impact energy of 40J for both central and dome sections of the vessel.

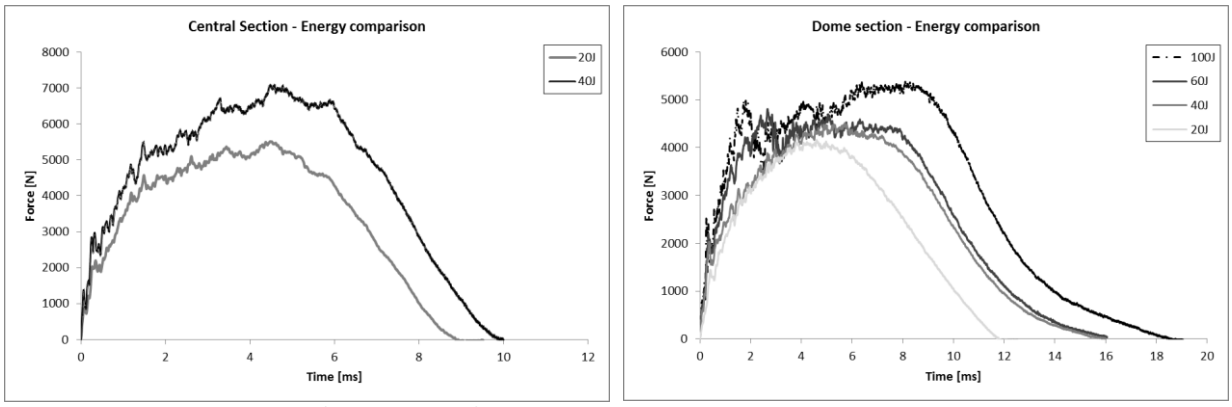

Figure 8: Experimental impact tests (averaged results)

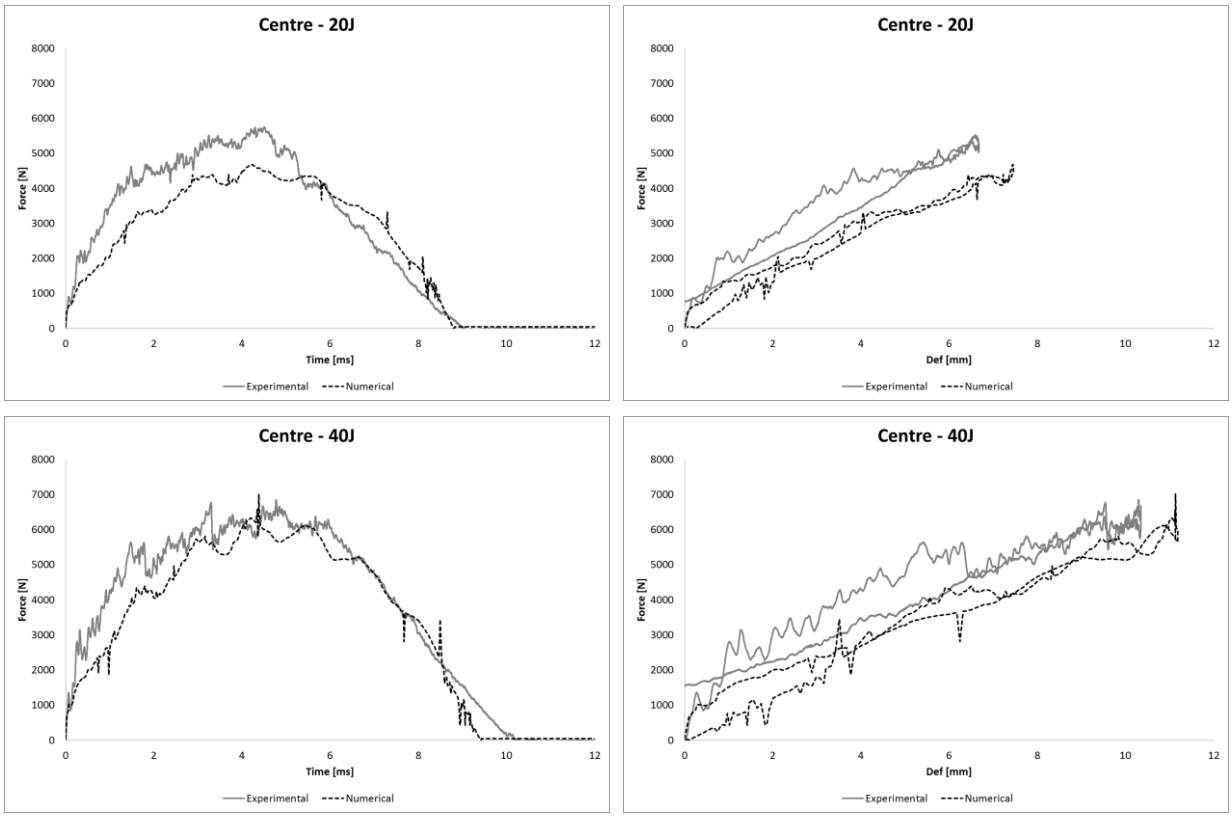

Figure 9: Num/Exp - Impact Central section - 20J

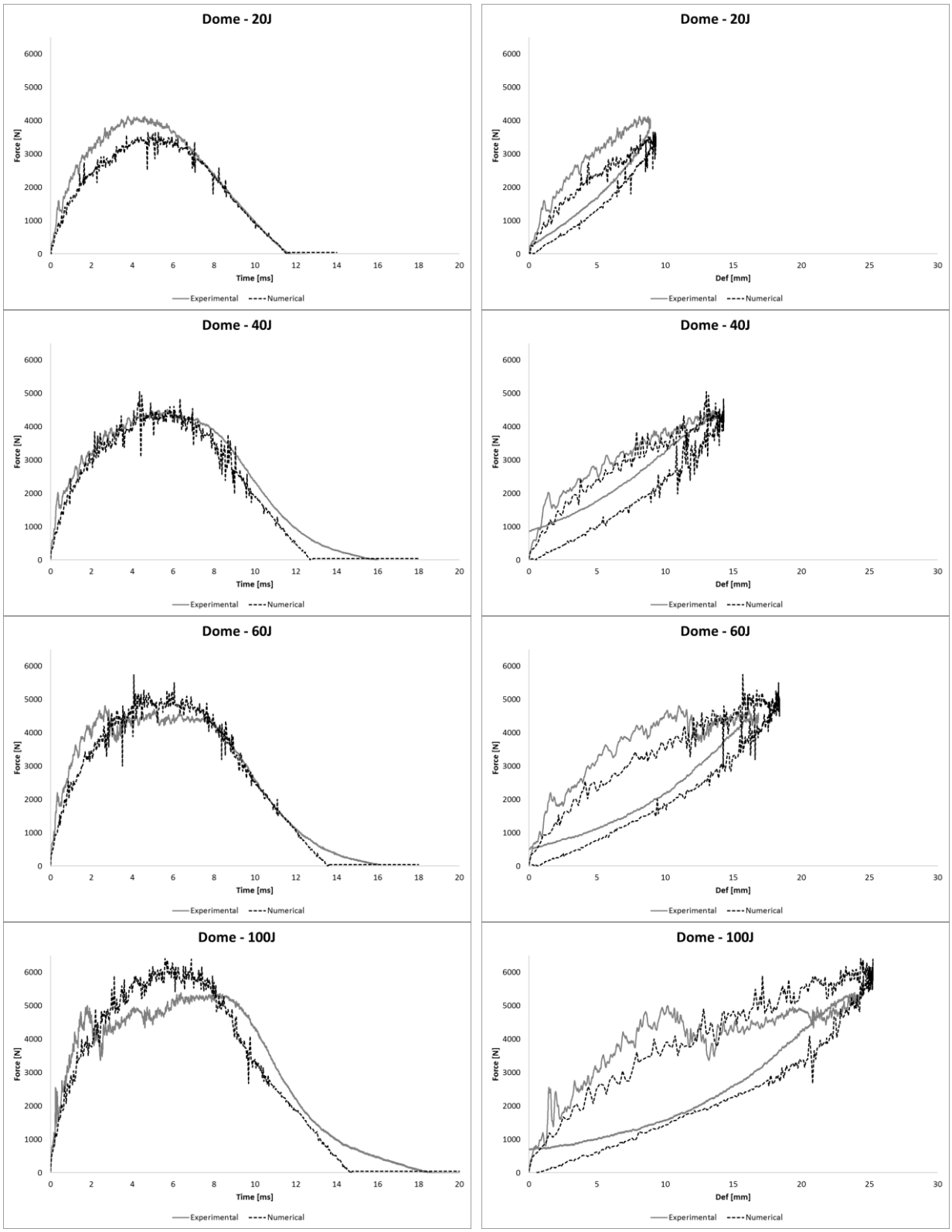

Figure 10: Num/Exp - Impact Dome section

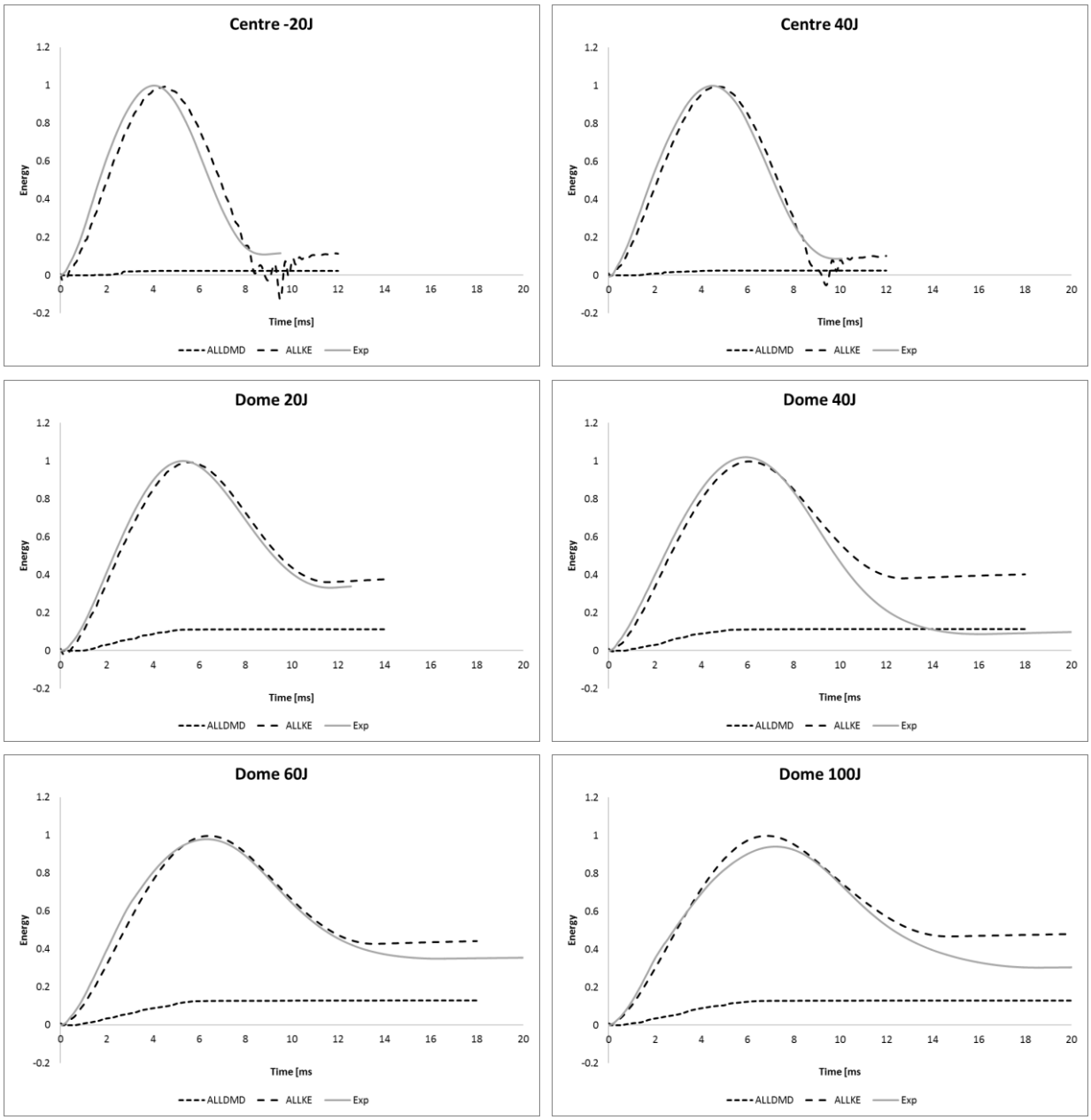

Figure 11: Num/Exp dimensionless energies comparison (ALLDMD: numerical damage energy, ALLKE: numerical kinetic energy, Exp: experimental kinetic energy

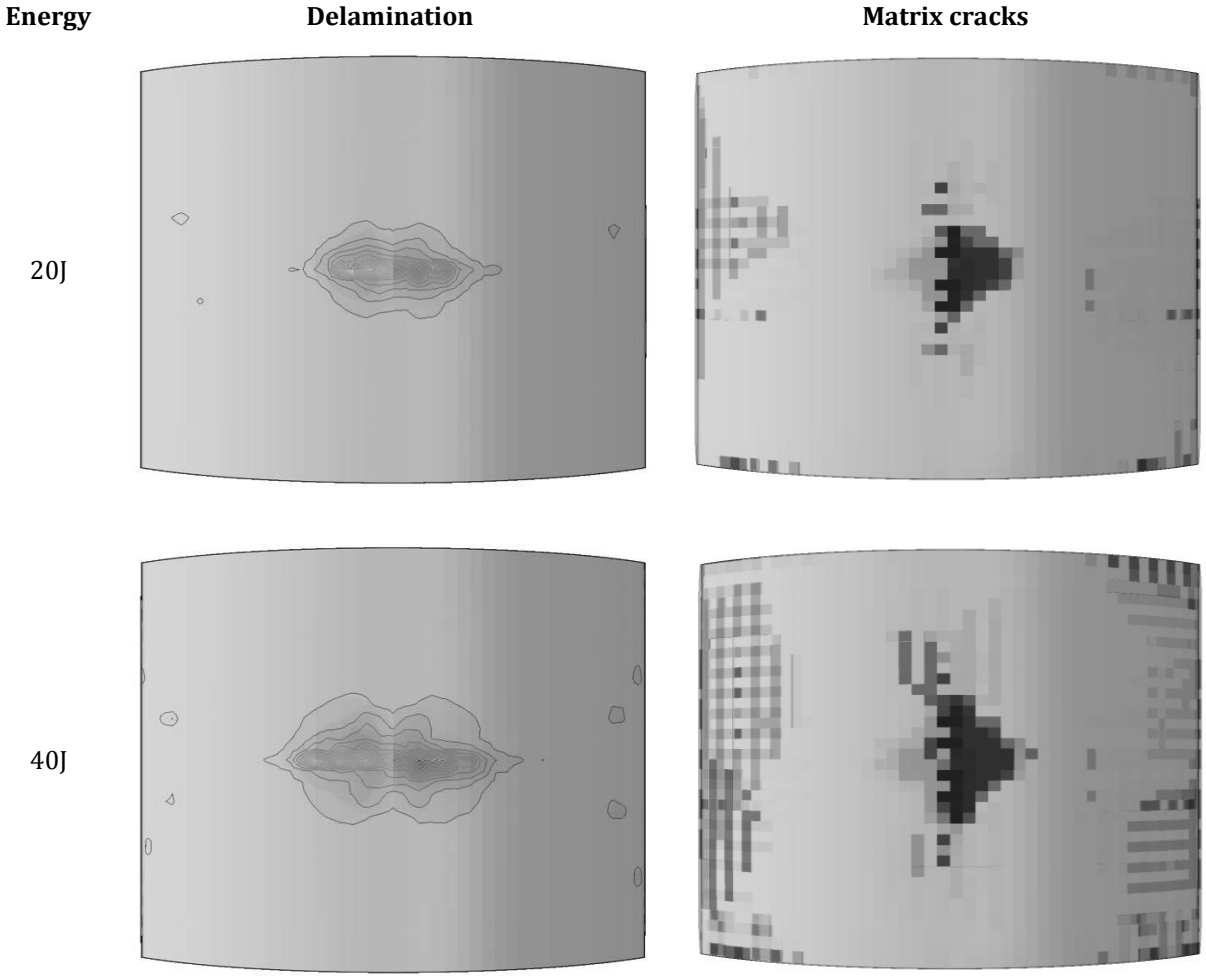

Figure 12: Impact on the central section - Numerical damages for the different impact energies. Colour scale varying from grey representative of no damage, to black for the full damage (all the element in the thickness direction)

Energy	Delamination	Matrix cracks
20J		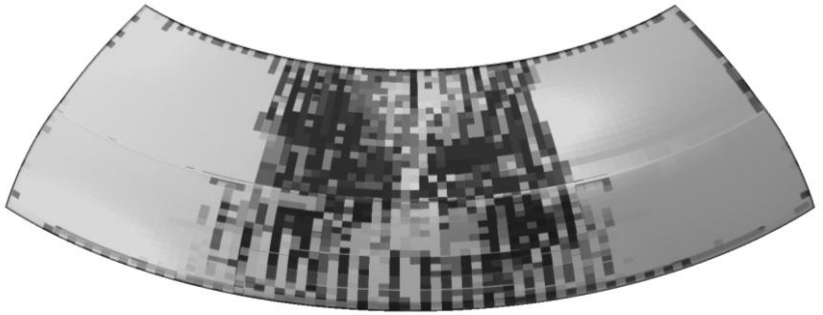
40J	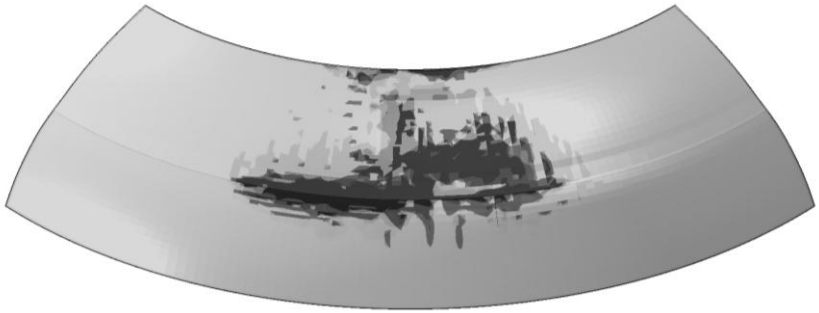	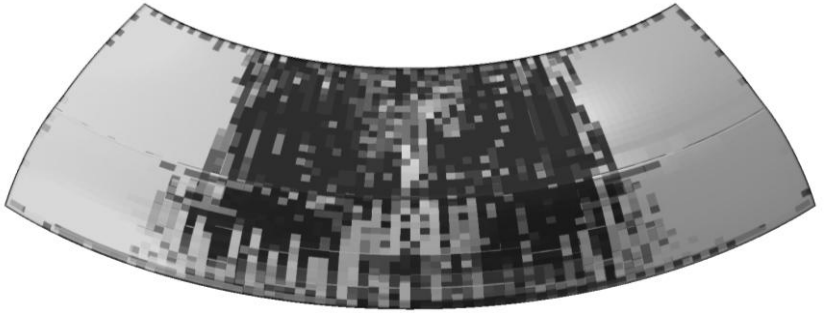
60J	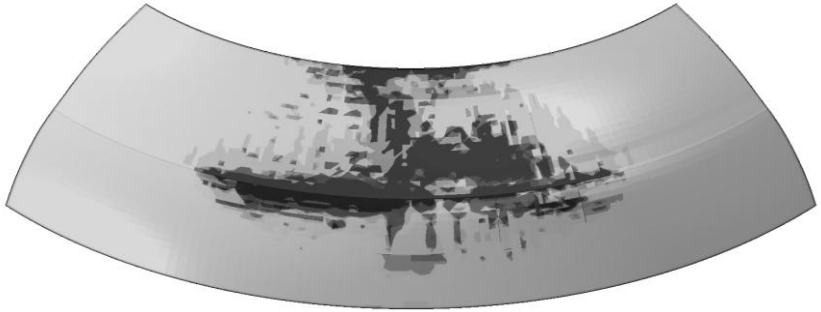	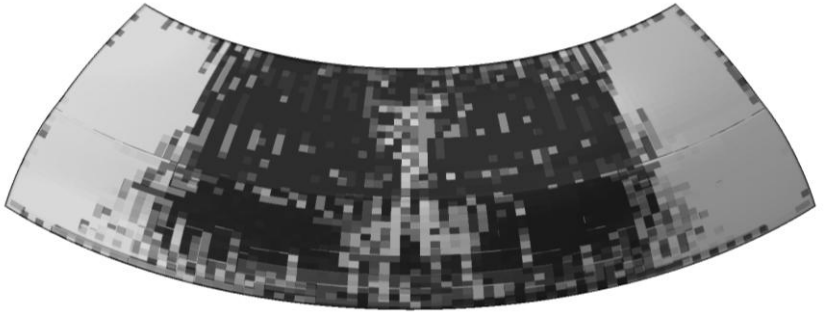
100J	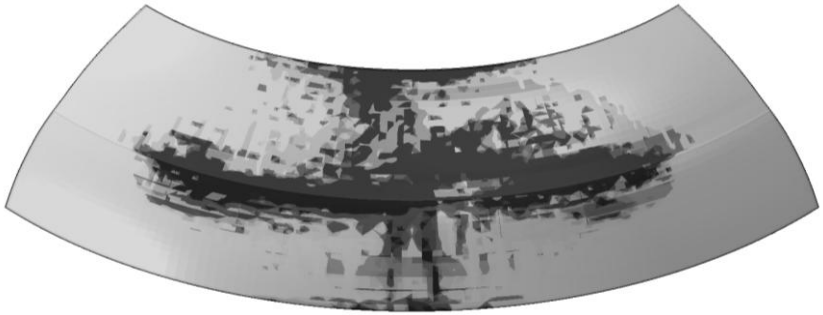	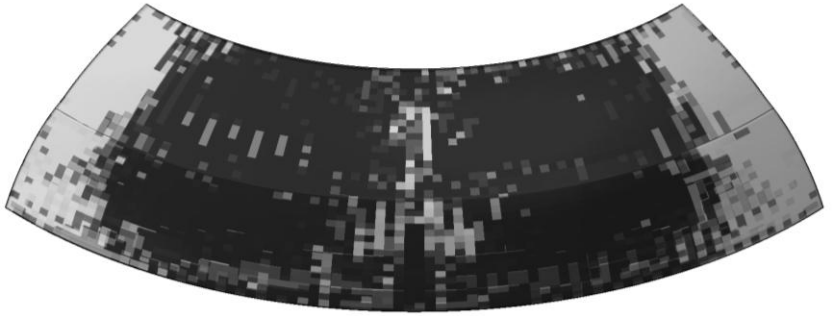

Figure 13: Impact on the dome section - Numerical damages for the different impact energies. Colour scale varying from grey representative of no damage, to black for the full damage (all the element in the thickness direction)